

# Path integral calculation for emergence of rapid evolution from demographic stochasticity

Hong-Yan Shih and Nigel Goldenfeld

*Department of Physics, Center for the Physics of Living Cells and Institute for Genomic Biology,  
University of Illinois at Urbana-Champaign, Loomis Laboratory of Physics,  
1110 West Green Street, Urbana, Illinois, 61801-3080*

Genetic variation in a population can sometimes arise so fast as to modify ecosystem dynamics. Such phenomena have been observed in natural predator-prey systems, and characterized in the laboratory as showing unusual phase relationships in population dynamics, including a  $\pi$  phase shift between predator and prey (evolutionary cycles) and even undetectable prey oscillations compared to those of the predator (cryptic cycles). Here we present a generic individual-level stochastic model of interacting populations that includes a subpopulation of low nutritional value to the predator. Using a master equation formalism, and by mapping to a coherent state path integral solved by a system-size expansion, we show that evolutionary and cryptic quasi-cycles can emerge generically from the combination of intrinsic demographic fluctuations and clonal mutations alone, without additional biological mechanisms.

PACS numbers: 87.23.-n, 87.18.Tt, 05.40.-a, 02.50.Ey

Predator-prey ecosystems exhibit noisy population oscillations whose origin is intuitively quite clear. The predator population number is activated by the prey, and so increases. This in turn inhibits the growth of the prey population, but the decline of the prey leads to a corresponding decline in the predator number too. As a result the prey population begins to rise, and the cycle begins again. The simplicity of this narrative belies the difficulty of making a quantitative model of ecosystems. Strong demographic fluctuations degrade the utility of population-level modeling, rendering it problematic to assess the appropriate scales for ecological modeling [1–6]. For example, observations of noisy periodicity in time series [7], slowly-decaying correlations [8] and spatiotemporal patterns [9] clearly reflect the stochastic nature of populations [10, 11] and their spatial organization. Moreover, even the simplest predator-prey systems exhibit complex spatial structure. This can arise through a variety of pattern formation processes [12–16] that include recent results on deterministic [17, 18] and fluctuation-induced Turing instabilities [9, 19, 20], traveling waves [16, 21, 22] and even analogies to the processes of phase separation in binary alloys [23]. In short, collective and stochastic many-body phenomena are ubiquitous in biology, and perhaps nowhere more so than in ecology.

The classical literature on predator-prey systems [24] assumes that evolution occurs on such long time scales that it can be neglected, but it is not obvious that this is always valid [25]. Recent work using rotifers (predator) and algae (prey) in a chemostat shows that dramatic changes in the population structure of the rotifer-algae predator-prey system can arise from rapid responses to intense selection among induced genetically distinct strains [26–33]. In these studies, so-called subpopulations with different traits emerge from evolution and lead to new trophic structures, accompanied by anomalous ecological dynamics. These anomalies include ‘evolutionary cycles’ with long oscillation periods in pop-

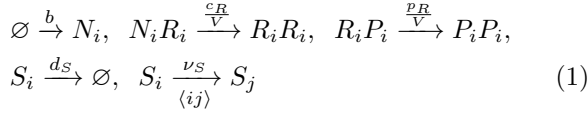
ulation dynamics and predator-prey phase shifts near  $\pi$  (and definitely distinct from the canonical value of  $\pi/2$ ), and ‘cryptic cycles’, in which prey populations remain almost constant while the predator population oscillates. Such phenomena have been modeled with deterministic differential equations containing empirical descriptions of functional response with a variety of detailed hypotheses on the mechanism of species interactions for rapid evolution [27–29, 32, 34–38] or non-heritable phenotypic plasticity [39]. Such models are not only very complex, with many adjustable parameters, but also cannot capture the stochasticity evident in the observations.

The purpose of this Letter is to propose and analyze a minimal model for rapid evolution that includes the effects of demographic stochasticity. Using tools from statistical mechanics, demographic stochasticity has been successfully captured using individual-level models (ILM) in a variety of situations that range from simple well-mixed predator-prey interactions [40–42] to spatially-extended systems that can exhibit quasi-Turing patterns [19, 20, 22, 43–45]. Here we propose an ILM for rapid evolution which we solve analytically by mapping the model into a coherent-state path integral representation [46–50] (for a review and history, see Ref. ([51])) followed by a volume expansion [52] to derive the effective Langevin equation for demographic fluctuations. Accompanied by Gillespie simulation [53] for the model, we show that this simple stochastic model can predict rapid evolution phenomena in well-mixed systems, yielding phase diagrams that are similar to those of more complex deterministic models and in qualitative agreement with available data. Thus key aspects of rapid evolution can be minimally modeled by subpopulation dynamics driven simply by intrinsic demographic stochasticity, without additional biological mechanisms. Our model can serve as a starting point for analyzing spatial distributions and large fluctuations such as extinction.

The physical explanation for anomalous cycles was un-

derstood early on [27]. In contrast to the  $\pi/2$  phase shift of the conventional predator-prey model, evolutionary cycles with  $\pi$  phase shift can arise because of the existence of a mutant prey population that can defend itself from the predator but which incurs a metabolic cost. The defended prey compete with the wild type for nutrients and thus delay the regrowth of the wild-type prey. The resulting additional phase lag of the wild-type prey behind the defended prey is about  $\pi/2$  because the wild-type prey must grow back before the population of the defended prey will return to its minimum level. When the defended prey have very effective defense without significant metabolic cost, there is substantial delay of the regrowth of the wild-type prey. If the wild-type prey lag the defended prey by  $\pi$ , their fluctuations offset each other, and thus the dynamics of the total prey population appears in aggregate to be suppressed, leading to the cryptic cycles.

*ILM for rapid evolution:* To model this quantitatively, consider a model for a system composed of nutrients for the prey (N), the vulnerable (wild-type) prey (W), the so-called ‘defended’ (mutant) prey (D), and the predator (P). The basic individual processes for them are regrowth of nutrients, reproduction of prey, predation by predator, death and migration to the nearest site for all individuals:



where  $\emptyset$  denotes the empty state,  $R = W, D$  is the prey index,  $S_i$  represents species  $S = N, W, D, P$  at site  $i$ , and  $V$  is an effective coarse-grained or correlation volume in which there is no significant population spatial variation. In ecology,  $V$  is called the patch size, and it acts as a control on the amplitude of demographic fluctuations. Because  $V$  is larger than the mean volume per organism, we will make analytical progress by using an expansion in inverse powers of  $V$ . The defended prey experiences a smaller predation rate than the wild-type prey, *i.e.*  $p_D < p_W$ , and also has a smaller reproduction rate or larger degeneration rate due to the metabolic cost for defense, *i.e.*  $c_W > c_D$  or  $d_W < d_D$ . For the nutrients,  $\nu_N$  and  $d_N$  are set to be zero. The corresponding master equation that defines the time evolution of the probability distribution of population states is

$$\begin{aligned} \partial_t P(\{n_{S_i}\}) &= \sum_{\{n_{S_i}\}} \left\{ b(E_{N_i}^{-1} - 1)(n_{N_i}^{\max} - n_{N_i}) \right. \\ &+ \sum_S d_S (E_{S_i} - 1) n_{S_i} + \sum_R \left[ \frac{c_R}{V} (E_{N_i} E_{R_i}^{-1} - 1) n_{N_i} n_{R_i} \right. \\ &\left. \left. + \frac{p_R}{V} (E_{R_i} E_{P_i}^{-1} - 1) n_{R_i} n_{P_i} \right] \right\} P(\{n_{S_i}\}), \end{aligned} \quad (2)$$

where  $\{\dots\}$  denotes the set over all sites and species, the prey index  $R = W, D$ , and the step operators  $E_{S_i}^{\pm}$  are defined as  $E_{S_i}^{\pm} f(\{n_{S_i}\}) = f(\{n_{S_i} \pm 1\})$ .

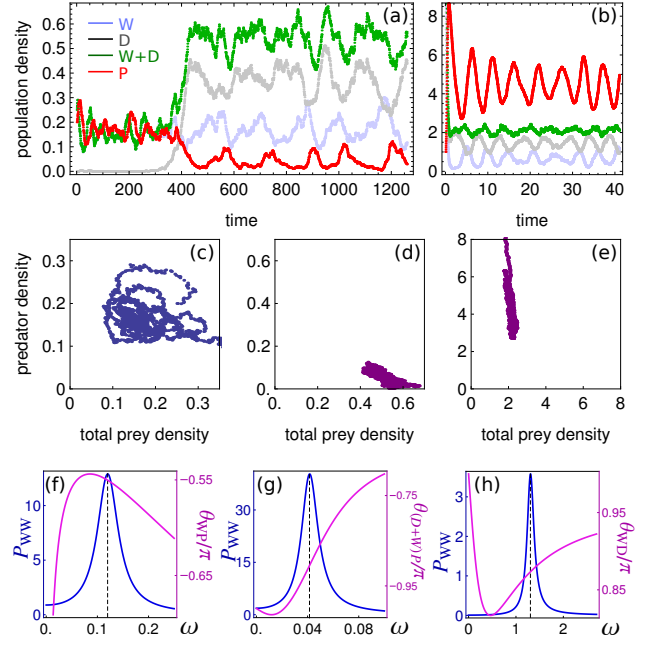


FIG. 1. Stochastic simulations for (a)evolutionary cycles emerging from normal cycles due to random mutation and for (b)cryptic cycles. Phase portraits of (c)normal cycles and (d)evolutionary cycles from the stochastic simulations show that the phase differences between predator and the total prey population are roughly  $\pi/2$  and  $\pi$  respectively, while for (e)cryptic cycles there is no obvious phase relationship. The estimated phase differences from analytic calculations based on ILM are  $-0.55\pi$  and  $0.905\pi$  for (f)normal cycles and (g)evolutionary cycles, and for (h)cryptic cycles the predicted phase difference between the wild-type prey and the defended prey is approximately  $0.874\pi$ . Parameter values are (a) $V = 1000$ ,  $c_W = 0.3$ ,  $p_W = 0.6$ ,  $c_D/c_W = 0.8$ ,  $p_D/p_W = 0.01$ ,  $d_D/d_W = 1$ ,  $\phi_{N,\max} = 1$ , and  $b = 0.1$ ; (b) $V = 380$ ,  $c_W = 60$ ,  $p_W = 0.92$ ,  $c_D/c_W = 0.95$ ,  $p_D/p_W = 0.001$ ,  $d_D/d_W = 7.5$ ,  $\phi_{N,\max} = 16$ , and  $b = 0.1$ .

*Spatial extension:* To complete the specification of the model, we need to include particle diffusion, for which the Doi formalism [46] is especially convenient. The resulting spatially-extended model represents a non-perturbative formulation of the model and can be used to study spatial patterns and large demographic fluctuations that are important near the ecosystem extinction transition, where the predator population vanishes [22]. The procedure is to write Eq. (2) as a second-quantized Hamiltonian and then express the generating functional for probabilities and correlations as a path integral [47, 48, 50, 51].

Following the standard procedure, we introduce the probability state vector in the Fock space constructed by different occupation number states:

$$|\psi\rangle = \sum_{\{n_{S_i}\}} P(\{n_{S_i}\}) |\{n_{S_i}\}\rangle, \quad (3)$$

so that the master equation becomes a Liouville equation

$$\partial_t |\psi\rangle = -\hat{H} |\psi\rangle, \quad (4)$$

with the Liouvillian  $\hat{H} = \sum_i \hat{H}_i$

$$\begin{aligned} \hat{H}_i = & b(1 - \hat{a}_{N_i}^\dagger)(n_{N_i}^{\max} - \hat{a}_{N_i}^\dagger \hat{a}_{N_i}) + \sum_R \left[ \frac{c_R}{V} (\hat{a}_{N_i}^\dagger \hat{a}_{N_i} \hat{a}_R^\dagger \hat{a}_{R_i} \right. \\ & \left. - \hat{a}_{N_i} \hat{a}_{R_i}^{\dagger 2} \hat{a}_{R_i}) + \frac{p_R}{V} (\hat{a}_{R_i}^\dagger \hat{a}_{R_i} \hat{a}_{P_i}^\dagger \hat{a}_{P_i} - \hat{a}_{R_i} \hat{a}_{P_i}^{\dagger 2} \hat{a}_{P_i}) \right] \\ & + \sum_S \left[ d_S (\hat{a}_{S_i}^\dagger \hat{a}_{S_i} - \hat{a}_{S_i}) + \nu_S \sum_{j \in N.N.} (\hat{a}_{S_i}^\dagger - \hat{a}_{S_j}^\dagger) \hat{a}_{S_i} \right] \quad (5) \end{aligned}$$

where  $\hat{a}_{S_i}^\dagger$  and  $\hat{a}_{S_i}$  are bosonic raising and lowering number operator for species  $S$  at site  $i$ . Eq. (4) and (5) are exact and naturally allow the representation of the many-body path integral formalism. Using the standard mapping to the coherent-state path integral representation and applying the volume expansion method, the effective Lagrangian density for Gaussian-order fluctuations becomes

$$\mathcal{L}^{(2)} = \tilde{\rho}^T \partial_t \boldsymbol{\xi} - \tilde{\rho}^T \mathbf{A}[\{\phi_S\}] \boldsymbol{\xi} - \frac{1}{2} \tilde{\rho}^T \mathbf{B}[\{\phi_S\}] \boldsymbol{\xi} \quad (6)$$

where  $\boldsymbol{\xi} = (\xi_N, \xi_W, \xi_D, \xi_P)$  and  $\tilde{\rho} = (\tilde{\rho}_N, \tilde{\rho}_W, \tilde{\rho}_D, \tilde{\rho}_P)$  are the fluctuation field vectors, and  $\mathbf{A}$  and  $\mathbf{B}$  are given in the Supplementary Material. Eq. (6) is equivalent to the Langevin equations as a function of wavenumber  $k$  and time:

$$\frac{d\boldsymbol{\xi}}{dt} = \mathbf{A}\boldsymbol{\xi} + \boldsymbol{\gamma}, \quad \langle \gamma_S(k, t) \gamma_{S'}(k', t') \rangle = \mathbf{B}_{SS'} \delta(k - k') \delta(t - t'). \quad (7)$$

In contrast to deterministic models [26–37, 39], the dynamics depends not only on the Jacobian  $\mathbf{A}[\{\phi_S\}]$  from the mean-field equation but also on the covariance matrix  $\mathbf{B}[\{\phi_S\}]$ . Since  $\mathbf{B}_{RR'}[\{\phi_S\}]$  in Eq. (7) is governed by the macroscopic densities, the white noise  $\boldsymbol{\gamma}$  that determines the dynamics of fluctuations is effectively multiplicative. Without the white noise  $\boldsymbol{\gamma}$ , the solutions for  $\boldsymbol{\xi}$  in the Langevin equations in Eq. (7) contributed by the linear terms are expected to decay exponentially and converge to mean-field densities  $\{\phi_S\}$ . However, the multiplicative white noise plays an important role: whenever it can cancel out the contribution of the eigenvalues of  $\mathbf{A}$ ,  $\boldsymbol{\xi}$  will be persistently driven away from convergent mean-field densities, *i.e.* white noise can select the frequency in the deterministic equations, resulting in periodic and strongly fluctuating population dynamics and spatial patterns. This is a resonant effect induced by demographic stochasticity through shot noise [40] with the resonant frequency near the slowest decaying mode in the mean-field solutions. Since the systems in the rotifer-algae experiments are well-mixed, the diffusion terms are neglected in the following calculation and simulation, but will be discussed elsewhere.

*Power spectrum, phase relationship and phase diagram:* The power spectrum of demographic noise has a resonant frequency corresponding to the deterministic eigenvalue. The power spectrum of species  $S$ ,  $P_{SS}(\omega)$ , can be calculated by taking the Fourier transform of the Langevin equations Eq. (7):

$$P_{SS'}(\omega) = \langle \tilde{\xi}_S(\omega) \tilde{\xi}_{S'}(-\omega) \rangle \quad (8)$$

with  $S' = S$ , and its Fourier transform gives the auto-correlation function. The phase difference between the fluctuation fields is defined as

$$\theta_{SS'}(\omega) = \tan^{-1} \frac{\text{Im}[P_{SS'}(\omega)]}{\text{Re}[P_{SS'}(\omega)]}. \quad (9)$$

For example, the phase difference between total prey and the predator,  $\theta_{(W+D)P}$ , can be calculated from  $P_{(W+D)P}(\omega) = \langle (\tilde{\xi}_W(\omega) + \tilde{\xi}_D(\omega)) \tilde{\xi}_P(-\omega) \rangle = P_{WP}(\omega) + P_{DP}(\omega)$ , which has the form of

$$P_{(W+D)P}(\omega) = \frac{\beta_6 \omega^6 + \beta_4 \omega^4 + \beta_2 \omega^2 + \beta_0}{\omega^8 + \alpha_6 \omega^6 + \alpha_4 \omega^4 + \alpha_2 \omega^2 + \alpha_0} \quad (10)$$

with a tail proportional to  $\omega^{-2}$ . The spectrum of phase difference between the predator and the total prey can be calculated from Eq. (9).  $P_{SS}(\omega)$  peaks at a resonant frequency which is smaller than the oscillation frequency of the deterministic solution because of the renormalization by the white noise in Eq. (7) [45]. The longer period reflects the presence of the defended prey that causes the delay of the regrowth of the wild-type prey and the predator.

Results of analytic calculations and simulations based on Eq. (1) are shown in Fig. 1. We use the Gillespie algorithm [53] for stochastic simulations and introduce random mutation from the wild-type prey to the defended prey. The mutation is added purely to seed a new sub-population to see the dramatic impact of the fixed sub-population after mutations, but plays no significant role in the subsequent dynamics; thus mutations are neglected in our analytical calculations below. We tried to simulate the experimental results of the rotifer-algae chemostat, where the control parameters are the nutrient concentration in flow media,  $\phi_N^{\max}$ , and the dilution rate,  $b$ . The natural degradation rates of the wild-type prey and predator are assumed to be much slower than the dilution rate, and therefore  $b \approx d_R \approx d_W < d_D$  (the defended prey is less healthy). In Fig. 1(a), at first there are only the wild-type prey and the predator in the system, and the dynamics exhibits normal cycles where the predator lags behind the prey by  $\pi/2$ . When predation pressure is high, around  $t \sim 400$ , a mutation has given rise to a defended prey population which subsequently adapts to dominate the population and cause additional delay in growth of the wild-type prey and the predator, leading to evolutionary cycles with  $\pi$  phase shift between the total prey and the predator. Fig. 1(b) shows an example of cryptic cycles, where the defended prey has similar reproduction rate as that of the wild-type prey, *i.e.*  $c_D \sim c_W$ , and the defended prey can advance the wild-type prey by nearly  $\pi$  and thus the total prey population is suppressed. The quasicycle calculations in Fig. 1(f)-(h) for power spectrum and phase spectrum in Eq. (8) with  $S = S'$  and Eq. (10) well predict the simulation results in Fig. 1(c)-(e). Besides the expected randomness in the dynamics from the stochastic simulation, Fig. 1(a) and (b) also show similar asymmetric profiles and

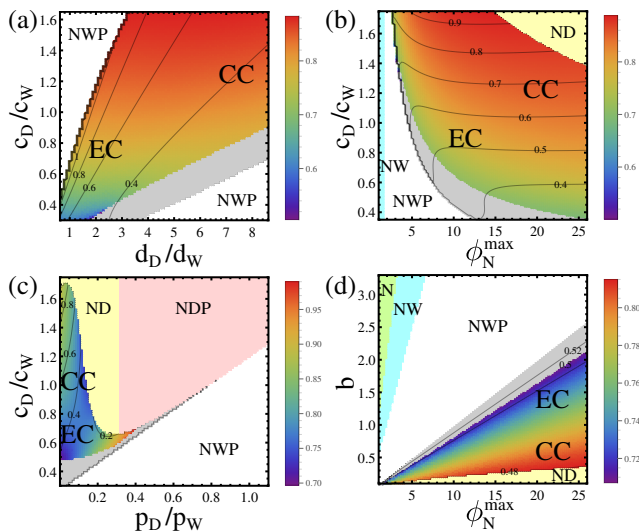


FIG. 2. Phase diagrams for evolutionary cycles (EC) and cryptic cycles (CC) calculated from ILM with respect to ratio of prey reproduction rate ( $c_D/c_W$ ), ratio of predation rate ( $p_D/p_W$ ), the maximum nutrient concentration ( $\phi_N^{\max}$ ) and the dilution rate ( $b$ ). The gradient-colorful region corresponds to the coexistence of the two types of prey and predator, and in the other regions the rapid evolution is not stable, with corresponding letters indicating the coexistence of only certain species. The color legend represents the predicted phase difference between the wild-type prey and the defended prey ( $\theta_{WD}$ ) for rapid evolution, in units of  $\pi$ . The contours are the estimated ratios of population fluctuations to mean-field solutions; when fluctuations are larger than mean-field solutions, the dynamics is under high risk of extinction. In the grey region near transition, the two types of prey start to decouple, leading to degenerate peaks in power spectra, and thus the phase is not well-defined. Except for the axis specified in each diagram, the parameters in calculations are  $V = 300$ ,  $c_W = 1$ ,  $p_W = 1$ ,  $c_D/c_W = 0.8$ ,  $p_D/p_W = 0.01$ ,  $r_D/r_W = 3.5$ ,  $\phi_N^{\max} = 16$ , and  $b = 0.6$ . The predicted phase diagram is consistent with stochastic simulation.

the longer period after the subpopulation emerges, as in the experimental data in [26–31, 33].

The phase diagram is usually studied by linear stability analysis of the mean field equations (for example, see Eq. (7)–(9) in the Supplementary Material). To reduce the dimension of parameter space, variables are rescaled to be dimensionless:  $\tilde{t} \equiv bt$ ,  $\tilde{d}_S \equiv d_S/b$ ,  $\tilde{\phi}_S \equiv \phi_S/\phi_N^{\max}$ ,  $\tilde{c}_S \equiv c_S\phi_N^{\max}/b$  and  $\tilde{p}_S \equiv p_S\phi_N^{\max}/b$ . However, this rescaling is rather subtle in stochastic calculations. For example, matrices  $\mathbf{A}$  and  $\mathbf{B}$  from Eq. (7) scale with  $1/\phi_N^{\max}$  as mean-fields  $\phi_S$ , but  $\gamma$  in Eq. (7) rescales with  $1/\sqrt{\phi_N^{\max}}$ , resulting in

$$\frac{\xi_S}{\phi_S} \sim \frac{1}{\sqrt{\phi_N^{\max}}} \frac{\tilde{\xi}_S}{\tilde{\phi}_S} \quad (11)$$

where  $\tilde{\xi}_S$  are the rescaled demographic noise fields. Therefore, for two stochastic individual-level models with the same mean-field limit after rescaling, demographic fluctuations are more important in the model

with smaller nutrient carrying capacity  $V\phi_N^{\max}$ . Thus neglecting fluctuations as in the conventional rescaling for mean-field equations can potentially cause unphysical predictions for the phase diagram. To avoid this situation, we examine the stability of solutions by comparing the amplitude of the lowest order population fluctuations with their mean fields.

Fig. 2 shows the calculated phase diagrams of ILM in Eq. (1). In Fig. 2(a), due to the cost for defense, the defended prey have inferior reproduction rate ( $c_D < c_W$ ) or are unhealthy than the wild-type prey ( $d_D > d_W$ ), leading to evolutionary cycles (EC). When the cost of reproduction is low, cryptic cycles (CC) can occur, where  $\theta_{WD} \approx \pi$ . If  $c_D$  is moderate, it is possible to have a correspondingly high death rate, and thus the fluctuations of prey are suppressed relative to the wild-type prey, causing the dynamics to be cryptic. In Fig. 2(b), under high  $\phi_N^{\max}$ , the defended prey are more likely to grow and dominate the system, which causes the wild-type prey to experience a greater phase lag than the defended prey, and the dynamics tends towards a completely cryptic cycle. In Fig. 2(c), if  $p_D$  is low, then higher  $c_D$  can lead to more phase delay and thus gives cryptic cycles. When  $p_D$  increases, the predator has greater food resource available from the defended prey, yielding a larger population, which then consumes more of the wild-type prey; this in turn reduces the wild-type prey population and leads to the dominance of the defended prey. In such a situation, the wild-type prey experiences a greater phase delay (nearly  $\pi$ ) behind the defended prey, but the wild-type prey population is too small to cancel out the fluctuations of the defended prey population, and thus the dynamics cannot be characterized as cryptic. Thus, by considering the amplitude of stochastic fluctuations, our result in Fig. 2(c) predicts a similar but slightly different phase diagram to Fig. 3 in [28]. In Fig. 2(d), under small  $b$ , *i.e.* slow supplement of the nutrient and low reduction rate from dilution, although both subpopulations of the prey have low reproduction, the wild-type prey population decreases more due to predation while the defended prey has a greater chance to compete for nutrient; thus the system is more likely to show cryptic cycles.

Our results show that rapid evolution strongly renormalize the ecosystem time scale, and the prediction of the coexistence region can help estimate the risk of extinction and the impact of the rate of environmental changes (for example, the dilution rate and nutrient concentration in the rotifer-algae system). Our model can also be used to study spatial-extended situations in natural ecosystems or lab experiments that are not in a well-mixed chemostat.

In summary, we have shown clearly that a generic stochastic individual-level model can yield rapid evolution phenomena, and that anomalous dynamics can arise without special assumptions or fine tuning, in sharp contrast to existing results in the ecology literature based on deterministic models. We expect this description to be especially useful to study the transition to rapid evolu-

tion from normal cycles, since before the transition the mutant prey population has low relative abundance and

is thus likely to exhibit strong effects of demographic stochasticity and spatiotemporal fluctuations.

- 
- [1] S. A. Levin, *Ecology* **73**, pp. 1943 (1992).
- [2] J. Bascompte and R. V. Solé, *Trends in Ecology & Evolution* **10**, 361 (1995).
- [3] M. Pascual and S. A. Levin, *Ecology* **80**, 2225 (1999).
- [4] M. Pascual, P. Mazzega, and S. A. Levin, *Ecology* **82**, pp. 2357 (2001).
- [5] N. Goldenfeld and C. Woese, *Annu. Rev. Condens. Matter Phys.* **2**, 375 (2011).
- [6] J. Chave, *Ecology Letters* **16**, 4 (2013).
- [7] C. Elton and M. Nicholson, *Journal of Animal Ecology* **11**, 215 (1942).
- [8] M. Pineda-Krch, H. J. Blok, U. Dieckmann, and M. Doebeli, *Oikos* **116**, 53 (2007).
- [9] J. A. Bonachela, M. A. Muñoz, and S. A. Levin, *Journal of Statistical Physics* **148**, 724 (2012).
- [10] M. B. Bonsall and A. Hastings, *Journal of Animal Ecology* **73**, 1043 (2004).
- [11] D. L. DeAngelis and W. M. Mooij, *Annual Review of Ecology, Evolution, and Systematics* , 147 (2005).
- [12] E. Meron, *Ecological Modelling* **234**, 70 (2012).
- [13] A. Liebhold, W. D. Koenig, and O. N. Bjørnstad, *Annual Review of Ecology, Evolution, and Systematics* , 467 (2004).
- [14] H. Malchow, F. M. Hilker, I. Siekmann, S. V. Petrovskii, and A. B. Medvinsky, in *Aspects of Mathematical Modelling* (Springer, 2008) pp. 1–26.
- [15] R. HilleRisLambers, M. Rietkerk, F. van den Bosch, H. H. Prins, and H. de Kroon, *Ecology* **82**, 50 (2001).
- [16] B. Blasius, A. Huppert, and L. Stone, *Nature* **399**, 354 (1999).
- [17] S. Levin and L. Segel, *Nature* **259**, 659 (1976).
- [18] S. Kinast, Y. R. Zelnik, G. Bel, and E. Meron, *Physical review letters* **112**, 078701 (2014).
- [19] T. Butler and N. Goldenfeld, *Phys. Rev. E Rapid Communications* **80**, 030902 (2009).
- [20] T. Butler and N. Goldenfeld, *Phys. Rev. E* **84**, 011112 (2011).
- [21] J. A. Sherratt, M. A. Lewis, and A. C. Fowler, *Proceedings of the National Academy of Sciences* **92**, 2524 (1995).
- [22] M. Mobilia, I. Georgiev, and U. Täuber, *Journal of Statistical Physics* **128**, 447 (2007).
- [23] Q.-X. Liu, A. Doelman, V. Rottschfer, M. de Jager, P. M. J. Herman, M. Rietkerk, and J. van de Koppel, *Proceedings of the National Academy of Sciences* **110**, 11905 (2013).
- [24] A. A. Berryman, *Ecology* **73**, 1530 (1992).
- [25] J. N. Thompson, *Trends in Ecology & Evolution* **13**, 329 (1998).
- [26] G. F. Fussmann, S. P. Ellner, K. W. Shertzer, and N. G. Hairston Jr., *Science* **290**, 1358 (2000).
- [27] T. Yoshida, L. E. Jones, S. P. Ellner, G. F. Fussmann, and N. G. Hairston, *Nature* **424**, 303 (2003).
- [28] T. Yoshida, S. P. Ellner, L. E. Jones, B. J. M. Bohannan, R. E. Lenski, and N. G. Hairston, Jr., *PLoS Biol* **5**, e235 (2007).
- [29] L. Jones and S. Ellner, *Journal of Mathematical Biology* **55**, 541 (2007).
- [30] L. Becks, S. P. Ellner, L. E. Jones, and N. G. Hairston Jr, *Ecology Letters* **13**, 989 (2010).
- [31] L. Becks, S. P. Ellner, L. E. Jones, and N. G. Hairston, *Ecology Letters* **15**, 492 (2012).
- [32] B. J. M. Bohannan and R. E. Lenski, *Ecology* **78**, 2303 (1997).
- [33] S. P. Ellner, *Functional Ecology* **27**, 1087 (2013).
- [34] K. W. Shertzer, S. P. Ellner, G. F. Fussmann, and N. G. Hairston, *Journal of Animal Ecology* **71**, 802 (2002).
- [35] A. Yamauchi and N. Yamamura, *Ecology* **86**, 2513 (2005).
- [36] M. H. Cortez and S. P. Ellner, *The American Naturalist* **176**, E109 (2010).
- [37] A. Mougi, *Theoretical Population Biology* **81**, 113 (2012).
- [38] A. Mougi, *Journal of Theoretical Biology* **305**, 96 (2012).
- [39] M. Yamamichi, T. Yoshida, and A. Sasaki, *The American Naturalist* **178**, 287 (2011).
- [40] A. J. McKane and T. J. Newman, *Phys. Rev. Lett.* **94**, 218102 (2005).
- [41] S. Morita, Y. Itoh, and K.-I. Tainaka, *Journal of the Physical Society of Japan* **74**, 819 (2005).
- [42] A. J. Black and A. J. McKane, *Trends in ecology & evolution* **27**, 337 (2012).
- [43] C. A. Lugo and A. J. McKane, *Physical Review E* **78**, 051911 (2008).
- [44] T. Butler and D. Reynolds, *Phys. Rev. E* **79**, 032901 (2009).
- [45] U. C. Täuber, *Journal of Physics A: Mathematical and Theoretical* **45**, 405002 (2012).
- [46] M. Doi, *Journal of Physics A: Mathematical and General* **9**, 1465 (1976).
- [47] P. Grassberger and M. Scheunert, *Fortschritte der Physik* **28**, 547 (1980).
- [48] A. Mikhailov, *Physics letters A* **85**, 214 (1981).
- [49] N. Goldenfeld, *Journal of Physics A Mathematical General* **17**, 2807 (1984).
- [50] L. Peliti, *Journal de Physique* **46**, 1469 (1985).
- [51] D. C. Mattis and M. L. Glasser, *Reviews of Modern Physics* **70**, 979 (1998).
- [52] N. van Kampen, *Canadian Journal of Physics* **39**, 551 (1961).
- [53] D. T. Gillespie, *The Journal of Physical Chemistry* **81**, 2340 (1977).

## SUPPLEMENTARY MATERIAL

### Appendix A: Path integral formalism for rapid evolution

By using the coherent-state representation, the Hamiltonian can be mapped onto the basis of coherent states and becomes a function of  $\alpha_S^*$  and  $\alpha_S$  which are the left and right eigenstates of  $\hat{a}_S^\dagger$  and  $\hat{a}_S$  respectively for species  $S = N, W, D, P$ . Since in general multiple individuals can occupy the same site in spatial extended systems,  $\hat{a}_S^\dagger$  and  $\hat{a}_S$  are considered to follow the bosonic commutation relation. The effective Lagrangian density in the path integral becomes

$$\mathcal{L} = \sum_i \left[ \alpha_S^* (\partial_t - \nu_S \nabla^2) \alpha_S + H(\{\alpha_S^*\}, \{\alpha_S\}) \right] \quad (\text{A1})$$

where  $\nu_N \equiv 0$ .

To study the fluctuations about the mean-field densities, it is convenient to map the system from field variables onto the physical variables by applying the semi-canonical Cole-Hopf transformation [22]

$$\alpha_S^* = e^{\tilde{\rho}_S}, \quad \alpha_S = \rho_S e^{-\tilde{\rho}_S} \quad (\text{A2})$$

where  $\rho_S$  are the population variables for species  $S$  and  $\tilde{\rho}_i$  are analogous to fluctuation variables. The Hamiltonian density under the transformation is obtained as

$$\begin{aligned} H = & b(1 - d^{\tilde{\rho}_N}) (n_{N,\max} - \rho_N) + \frac{c_R}{V} (1 - e^{\tilde{\rho}_R - \tilde{\rho}_N}) \\ & + \frac{p_R}{V} (1 - e^{\tilde{\rho}_P - \tilde{\rho}_R}) + d_R \rho_R (1 - e^{-\tilde{\rho}_R}) \\ & + d_P \rho_P (1 - e^{-\tilde{\rho}_P}). \end{aligned} \quad (\text{A3})$$

Further we apply the ansatz[44]

$$\tilde{\rho}_S \rightarrow \frac{\tilde{\rho}_S}{\sqrt{V}}, \quad \rho_S = V \phi_S + \sqrt{V} \xi_S, \quad (\text{A4})$$

where  $\langle \tilde{\rho}_S \rangle$  are the mean-field population density variables and the deviations around them,  $\phi_S$ , are of order  $1/\sqrt{V}$ . The patch size  $V$  becomes the system size in the well-mixed case. This expansion will lead to a lowest order of fluctuations in Gaussian form. After applying the expansion in Eq. (A4), the Lagrangian density in Eq. (A1) can be separated into different orders of  $\sqrt{V}$

$$\mathcal{L} = \sqrt{V} \mathcal{L}^{(1)} + \mathcal{L}^{(2)} + \dots \quad (\text{A5})$$

Here

$$\begin{aligned} \mathcal{L}^{(1)} = & \sum_S \tilde{\rho}_S \partial_t \phi_S + b \phi_N \tilde{\rho}_N + \sum_R \left[ -\nu_R \tilde{\rho}_R \nabla^2 \phi_R \right. \\ & + c_R \phi_N \phi_R (\tilde{\rho}_N - \tilde{\rho}_R) + p_R \phi_R \phi_P (\tilde{\rho}_R - \tilde{\rho}_P) \\ & \left. + d_R \phi_R \tilde{\rho}_R \right] + d_P \phi_P \tilde{\rho}_P - \nu_P \tilde{\rho}_P \nabla^2 \phi_P. \end{aligned} \quad (\text{A6})$$

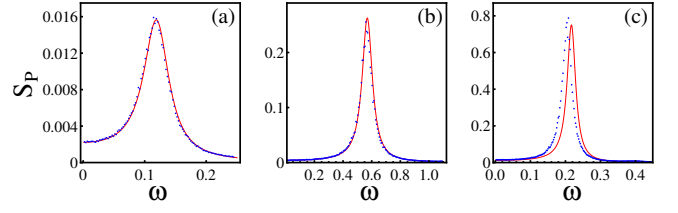


FIG. 3. Examples of comparison between analytic calculation (red curve) and stochastic simulation (blue dots) of power spectrum of population fluctuations of predator for (a) normal cycles, (b) evolutionary cycles and (c) cryptic cycles in individual level model. The parameters in calculations and simulations are (a)  $V = 2000$ ,  $b = 0.1$ ,  $c_W = 0.3$ ,  $p_W = 0.6$ ,  $\phi_N^{\max} = 1$ , (b)  $V = 1600$ ,  $b = 0.6$ ,  $c_W = 1$ ,  $p_W = 1$ ,  $\phi_N^{\max} = 5$ ,  $c_D/c_W = 1.6$ ,  $p_D/p_W = 0.001$ ,  $r_D/r_W = 3.5$  and (c)  $V = 1600$ ,  $b = 0.1$ ,  $c_W = 60$ ,  $p_W = 0.92$ ,  $\phi_N^{\max} = 16$ ,  $c_D/c_W = 0.95$ ,  $p_D/p_W = 0.001$ ,  $r_D/r_W = 7.5$ .

The stationary solution from  $\frac{\delta \mathcal{L}_1}{\delta \tilde{\rho}_S} = 0$  gives the mean-field dynamics:

$$\partial_t \phi_N = b(\phi_{N,\max} + \phi_N) - c_R \phi_N \phi_R, \quad (\text{A7})$$

$$\partial_t \phi_R = \nu_R \nabla^2 \phi_R + c_R \phi_N \phi_R - p_R \phi_R \phi_P + d_R \phi_R, \quad (\text{A8})$$

$$\partial_t \phi_P = \nu_P \nabla^2 \phi_P + p_R \phi_R \phi_P - d_P \phi_P. \quad (\text{A9})$$

The Lagrangian density in the next order is

$$\mathcal{L}^{(2)} = \tilde{\rho}^T \partial_t \xi - \tilde{\rho}^T \mathbf{A}[\{\phi_R\}] \xi - \frac{1}{2} \tilde{\rho}^T \mathbf{B}[\{\phi_S\}] \xi, \quad (\text{A10})$$

where  $\xi = (\xi_N, \xi_W, \xi_D, \xi_P)$  and  $\tilde{\rho} = (\tilde{\rho}_N, \tilde{\rho}_W, \tilde{\rho}_D, \tilde{\rho}_P)$  are the fluctuation field vectors, and

$$\begin{aligned} \mathbf{A}_{NN} &= -b - c_R \phi_R, \quad \mathbf{A}_{NR} = -\mathbf{A}_{RN} = -c_R \phi_N, \\ \mathbf{A}_{NP} &= \mathbf{A}_{PN} = \mathbf{A}_{WD} = \mathbf{A}_{\nu_R} = 0, \\ \mathbf{A}_{RR} &= -\nu_R k^2 + c_R \phi_R - p_R \phi_P - d_R, \\ \mathbf{A}_{RP} &= -\mathbf{A}_{PR} = -p_R \phi_R, \quad \mathbf{A}_{PP} = -\nu_P k^2 + p_R \phi_R - d_P, \\ \mathbf{B}_{NN} &= b(\phi_N^{\max} - \phi_N) + c_R \phi_N \phi_R, \\ \mathbf{B}_{NR} &= \mathbf{B}_{RN} = -c_R \phi_N \phi_j, \\ \mathbf{B}_{NP} &= \mathbf{B}_{PN} = \mathbf{B}_{WD} = \mathbf{B}_{DW} = 0, \\ \mathbf{B}_{RR} &= \nu_R \phi_R k^2 + c_R \phi_N \phi_R + p_R \phi_R \phi_P + d_R \phi_R, \\ \mathbf{B}_{RP} &= \mathbf{B}_{PR} = -p_R \phi_R \phi_P, \\ \mathbf{B}_{PP} &= \nu_P \phi_P k^2 + p_R \phi_R \phi_P + d_P \phi_P. \end{aligned} \quad (\text{A11})$$

Following the Martin-Siggia-Rose response function formalism, the next order  $\mathcal{L}^{(2)}$  generates a Langevin equation capturing the dynamics with Gaussian fluctuations. However, it is important to emphasize that the Gaussian noise here should not be additive but is multiplicative because these fluctuations originate from the demographic stochasticity of the population at each time step, resulting in quasicycles induced by a resonant amplification of intrinsic fluctuations [40], and leading to a longer tail in distribution distinct from limit cycles [20].



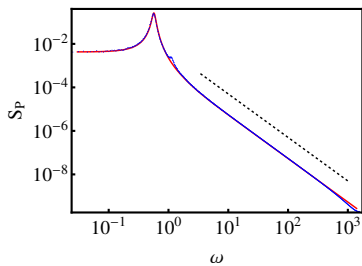


FIG. 4. The logarithm scale of comparison of power spectrum between analytic calculation and stochastic simulation in Fig 3(b). The tail with  $\omega^{-2}$  scaling, indicated by a reference dotted line with slope of  $-2$ , is the signature of quasicycles and is predicted by the analytic calculation based on individual level model.

### Appendix B: Comparison between analytic calculation and stochastic simulation

We have computed the power spectra, and compared the results with the stochastic simulation. The power spectrum for species  $S$  is calculated analytically by  $S_S(\omega) = P_{SS}(\omega) = \langle \tilde{\xi}_S(\omega) \tilde{\xi}_S(-\omega) \rangle$ , and from Gillespie stochastic simulations of the ILM, using the formula

$$S_S(\omega) = \frac{1}{T} \langle \tilde{\xi}'_S(\omega_m) \tilde{\xi}'_S(-\omega_m) \rangle, \quad (\text{B1})$$

where  $T = t_0 + N\Delta t$  is the duration of total  $N$  samplings with discrete time  $t_n = t_0 + n\Delta t$  and the discrete Fourier transform of  $\xi$  is defined as

$$\begin{aligned} \tilde{\xi}'(\omega_m) &= \sum_{n=1}^N \xi(t_n) e^{i\omega_m t_n} \Delta t \\ &= \frac{T}{N} \sum_{n=1}^N \xi(t_n) e^{i2\pi(m-1)(n-1)/N}. \end{aligned} \quad (\text{B2})$$

The peaks and magnitudes of the power spectra of calculation and simulation have good agreement when the Gaussian approximation is valid. There are slight deviations when either the wild-type prey or predator has a small population size. In such a case, the dynamics of fluctuations is dominated by the species with smaller population, leading to a skewed and leptokurtic distribution of population fluctuations. Such suppressed fluctuation distribution can explain the deviation of the power spectra of simulation data from the analytic calculation when there is large discrepancy in population sizes between species. Fig. 3 shows examples of comparison between analytic calculation and stochastic simulation for normal cycles, evolutionary cycles and cryptic cycles. When population sizes are similar for each species and are not small, analytic calculation based on Gaussian fluctuations provides good quantitative prediction of characteristic frequency and the shape of power spectrum. Fig. 4 shows the  $\omega^{-2}$  scaling in power spectrum as the signature of quasicycles is also captured by analytic calculation. For cryptic cycles where the oscillations of predator population are relatively larger and the prey population size is usually smaller, the Gaussian approximation is expected to have less quantitative agreement and underestimate the amplitude of fluctuations as shown in Fig. 3(c).